Scientia Iranica B (2016) 23(5), 2097–2112

Sharif University of Technology
Scientia Iranica
Transactions B: Mechanical Engineering
www.scientiairanica.com

Features of flow past a circular cylinder with a slit

W. Jian Sheng[a] and W. Chen[b,*]

a. *Key Laboratory of Efficient Utilization of Low and Medium Grade Energy, MOE, School of Mechanical Engineering, Tianjin University, Tianjin 300072, China.*
b. *School of Mechanical Engineering, Department of Mechanics, Tianjin University, Tianjin 300072, China.*

Received 20 May 2014; received in revised form 29 January 2015; accepted 16 August 2016

KEYWORDS
Passive control;
Cylinder with a slit;
Vortex suppression;
Drag and lift coefficients;
Strouhal number.

Abstract. The impact of a slit placed along a circular cylinder diameter, which is parallel to the incoming flow, is numerically investigated in order to find a geometric modification that can help drag reduction, as well as vortex suppression, without any additional energy consumption. The drag reduction is achieved by diverting part of the fluid in the front stagnation region into the low pressure zone at the back of cylinder through the slit. The Reynolds number based on the cylinder diameter, D, ranges from 60 to 250. The effect of the slit width ratio (s/D) on the drag and lift coefficients, the Strouhal number, and the wake flow feature of the cylinder is presented. Favorable reduction of drag and lift coefficients is observed with the rising of slit width ratio. The vortex shedding generated from the slit alters the wake flow thoroughly and drives the vortex shedding derived from the cylinder surface to further downstream.

1. Introduction

The viscous flow past a circular cylinder has been widely studied for its geometric simplicity and representative feature of general bluff body wakes [1-3]. A significant feature of the flow is the Karman vortex street, which began with the pioneering work of von Karman. The pressure on the surface of the cylinder varies as vortices are shed alternatively from both sides of cylinder. The vortex shedding appears together with fluctuation of drag and lift forces, which may result in generation of vibrations and noises, thus shortens the life of structure [4,5]. Further research of strategies to control flow past bluff bodies can be used in fields such as drag reduction, lift enhancement, noise and vibration control. Therefore, finding an effective way for controlling the bluff body wake is significantly important in the view of practical engineering [6]. A lot of controlling ways have been purposed over the past decades. In general, control methods of wake flow can be divided into active and passive methods. Active control is achieved by supplying external energy, such as the rotating cylinder [7], suction and blowing [8,9], oscillating foil [10], momentum injection [11], the insertion of additional vortices in the flow [12], cylinder vibrations [13], acoustic forcing [14], time harmonic forcing [15], and ribbon techniques [16,17]. Additional power input is needless for the passive way. Due to the fact that active method requires complex devices that provide external power for the flow, the passive method is simpler and less costly to be implemented. Passive method is applied by modifying the surface of attaching additional devices like splitter plate [18], control rods [19], screen [20], parallel dual plates [21], wall near the cylinder [22], base bleed [23], and small secondary cylinder [24], or shape modifications like grooved or wavy cylinders, etc. [25-28]. The works above show that wake structure can be controlled passively through changing the surface structure or attaching additional devices to the bluff body.

The purpose of this paper is to propose a method to restrain vortex shedding by using passive method of

*. *Corresponding author.*
E-mail address: chenwang_tju@163.com (W. Chen)

modifying the circular cylinder shape, that is, placing a two-dimensional (2D) slit parallel to flow along the cylinder diameter. The idea of slit control comes from the standpoint of decreasing the pressure difference between the higher pressure in the front stagnation zone and the lower one in the rear separated zone by diverting part of the fluid from the front stagnation point to the rear one through the slit, resulting in the reduction of the total drag force. There are also some industry applications making use of the cylinder-slit configuration. As for a circular cylinder with a slit parallel to the flow direction, it can be regarded as a bluff-body flame-holder for stabilizing the flame [29]. On the other hand, for a circular cylinder having a slit perpendicular to the flow direction, it can serve as a Karman vortex flow meter [30].

As far as the authors know, the control model of a circular cylinder with a slit has been proposed in limited quantity of references, and a thorough study of the impact of the slit width on the wake flow has not been performed yet. Igarashi [31] studied experimentally the effect of the angle of the slit placing along the cylinder diameter on the wake flow. It is found that a slit with angle less than 40° drives the vortex generation zone towards downstream and augments the base pressure, while slit with angle larger than 60° decreases both the base pressure and shedding frequency due to the intensified separated vortices. The effect of the slit is slight when the slit angle varies from 40° to 60°. Meanwhile, Olsen and Rajagopalan [32] conducted an experimental investigation of modified cylinders, including those with slit or concave rear notch, or both. The flow past two adjacent circular cylinders is similar to our work. Zdravkovich [33,34] reviewed the flow interference when two cylinders are placed adjacently in tandem and staggered ways. It is found that the resulting forces and vortex shedding pattern may differ from those of single body, when multiple bluff bodies are immersed in a flow. In adjacent arrangements of cylinder, experimental work [35-38] showed that the flow could be summarized into two regimes, and a complex transition region exists between them. As the two cylinders are located very closely, the flow is periodic and the wake is a Karman vortex street as if the flow past a single bluff body. When the distance between two cylinders becomes longer, coupled and synchronized vortex streets are observed. Intermediate spacing leads to very complex transitional patterns, like bi-stable biased gap flow observed by Kim and Durbin [39]. Also, relevant investigations on the flow control include suction or blowing on a bluff body, such as Wood [40], Lin et al. [41], and Kim and Choi [42]. A recent study of Baek and Karniadakis [43] investigated numerically the Vortex-Induced Vibrations (VIV) control via a slit, and they observed that a slit parallel to the flow direction could both weaken and detune the vortex shedding, which is effective in suppressing the VIV.

The goal of the present work is to study the effect of the slit width on the wake flow, which is located along the cylinder diameter parallel to the flow direction, which is expected to be an efficient control method for manipulating cylinder wake flow by suppressing the vortex shedding. The present work, differing from the previous study, is the investigation on the mechanism of drag reduction with a series of modified circular cylinder in a reliable two-dimensional regime. The effect of parameters like slit width and Reynolds number on wake structure, characteristic parameters, especially the vortex shedding and drag reduction, is probed. It is predicted to find the modified circular cylinder with the lowest drag coefficient.

In the present work, six configurations are used: one unmodified circular cylinder and five modified circular cylinders with different slit widths (s). The Reynolds number based on the cylinder diameter ranges from 60 to 250. For flow past a circular cylinder, it is well known that the vortex shedding appears at $\mathrm{Re} \sim 47$ [44] as a result of the first instability in the wake. The above unsteady wake flow is also called 2D laminar wake regime or periodic one. The flow remains two-dimensional up to $\mathrm{Re} \approx 190$. For Re larger than 190, wake regime transforms from two- to three-dimensionality and the wake becomes strongly three-dimensional at $\mathrm{Re} = 260$ [45]. At Reynolds numbers of approximately 200 or less, the Strouhal number and fluctuating forces over a circular cylinder using two-dimensional models are obtained [46,47]. When Reynolds numbers are high, 2D models cannot precisely predict the lift and drag forces due to the presence of three-dimensionality of the flow field. Nevertheless, it is still worthwhile to probe the capabilities and limitations of the 2D numerical process at higher Reynolds numbers, which requires significantly less cost than that of three-dimensional process does. Therefore, two-dimensional simulations are performed in the present work to probe and characterize the effectiveness of the cylinder-slit, which may provide a deeper insight for the physics mechanism. Analysis of the results is accomplished by presenting the fluctuating lift and drag coefficients, shedding Strouhal number, and the features of the wake flow at various slit width ratios.

2. Numerical processes

2.1. Governing equations

The governing equations of the flow regime considered in the present work are the equation of continu-

ity and time-dependent incompressible Navier-Stokes equations. The governing equations of two-dimensional incompressible fluid are described as follows:

The continuity equation:

$$\frac{\partial u}{\partial x}+\frac{\partial v}{\partial y}=0. \quad (1)$$

The momentum equation in the streamwise and cross-flow directions are:

$$\frac{\partial u}{\partial \tau}+u\frac{\partial u}{\partial x}+v\frac{\partial u}{\partial y}=-\frac{1}{\rho}\frac{\partial p}{\partial x}+v\left(\frac{\partial^2 u}{\partial x^2}+\frac{\partial^2 u}{\partial y^2}\right), \quad (2)$$

$$\frac{\partial v}{\partial \tau}+u\frac{\partial v}{\partial x}+v\frac{\partial v}{\partial y}=-\frac{1}{\rho}\frac{\partial p}{\partial y}+v\left(\frac{\partial^2 v}{\partial x^2}+\frac{\partial^2 v}{\partial y^2}\right). \quad (3)$$

2.2. Computational domain and mesh features

Flow past a rigid two-dimensional circular cylinder at a range of Reynolds numbers from 60 to 250 is considered. In the present work, the Reynolds number is given by $U_\infty D/\nu$. The diameter of the cylinder used in the present work is 40 mm. The computational domain extends from $-10D$ at the inlet to $20D$ at the outlet and extends from $-10D$ to $10D$ in the cross-flow direction. The coordinate origin is located at the center of the cylinder, and the positive x-axis points downstream. The mesh near the cylinder wall should be dense enough to capture the behavior of the boundary layer, which plays an important role in predicting the forces acting on the cylinder surface. To facilitate meshing and speed up the simulation, the whole computational domain is divided into nine parts, as shown in Figure 1(a). A square with a side length of six times the cylinder diameter (zone 5) is created around the cylinder, and quadrilateral mesh is used. The dense structured mesh is employed in four zones adjacent to zone 5 (zones 2, 4, 6, and 8), and unstructured mesh is used in other four zones (zones 1, 3, 7 and 9). Mesh generation is initially completed in the square domain containing the cylinder (zone 5), and other zones will be meshed based on the initial grids. A typical 2D computational domain is displayed in Figure 1(b). A 60×60 quadrilateral mesh is chosen in zone 5, and the cylinder surface is divided into 240 cells, as shown in Figure 1(c). To testify the mesh resolution of computational domain, grid convergence test is carried out for flow past an unmodified circular cylinder at Re = 180. Mesh sensitivity analysis is performed by varying the mesh density in zone 5 and at the cylinder surface to assess its effect on the mean drag coefficient, as discussed in Section 3.1. The flow configuration of a circular cylinder with a slit placed parallel to the flow direction along the cylinder diameter is sketched in Figure 2(a). Parameter s represents the width of the slit and varies from 0

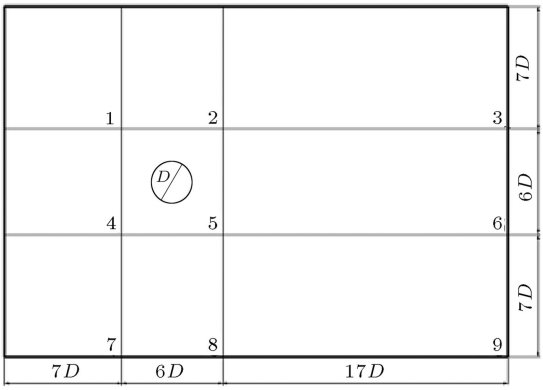

(a)

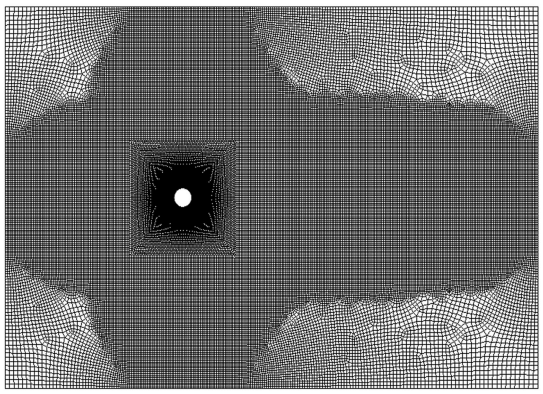

(b)

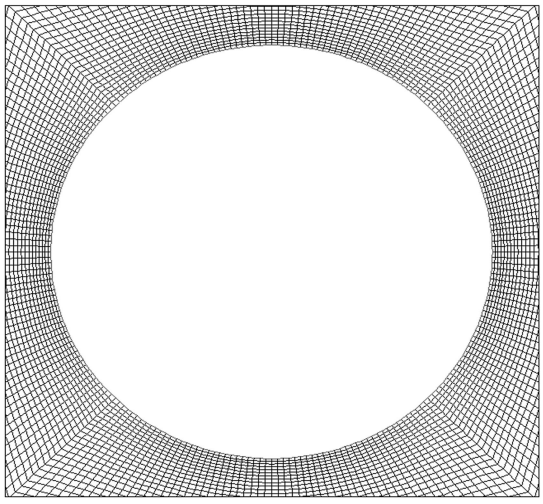

(c)

Figure 1. (a) Sketch of the division of the computational domain. (b) Meshing of the computational domain. (c) Structured meshing around the cylinder (zone 5).

to $0.3D$ in the simulation. Computational domain near the cylinder wall is displayed in Figure 2(b). Quadrilateral meshes are also adopted in the slit and the cylinder surface.

In the Reynolds number range considered, the alternative vortex shedding will result in periodical fluctuating forces on the cylinder wall. The forces

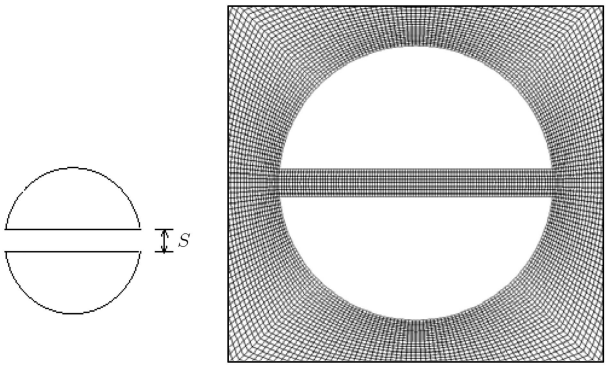

Figure 2. (a) Sketch of circular cylinder with a slit. (b) Structured meshing in the slit and around the cylinder.

acting on the circular cylinder are obtained as follows:

$$F_D = \int_0^{2\pi} (-p\cos\theta + \tau_w \sin\theta) R d\theta, \tag{4}$$

$$F_L = \int_0^{2\pi} (-p\sin\theta - \tau_w \cos\theta) R d\theta. \tag{5}$$

F_D and F_L are the total drag and lift forces, respectively. $R(= D/2)$ represents the radius of cylinder. The first terms of both Eq. (4) and (5) are the components of the pressure, while the second terms are components of the shear stress. As for the cases of modified cylinders, the forces exerted on the two circular curve surfaces could be calculated by changing the domain of the integration and contribution of the pressure; shear force acting on the slit walls should also be considered. The drag and lift forces are nondimensionalized by $\rho U^2 D/2$, thus the drag and lift coefficients C_D and C_L are described as follows:

$$C_D = \frac{F_D}{\rho U_\infty^2 D/2}, \tag{6}$$

$$C_L = \frac{F_L}{\rho U_\infty^2 D/2}. \tag{7}$$

The non-dimensional shedding frequency, Strouhal number, is defined as:

$$\mathrm{St} = \frac{f_s D}{U_\infty}, \tag{8}$$

where it could be calculated by the Fast Fourier Transform (FFT) of the lift force component. Because the lift and drag forces are caused by the periodic upper and lower sheddings of the vortex, the lift and drag forces will be periodically oscillating in a fully developed flow past the circular cylinder and the time-averaged lift coefficient becomes zero without control. It is remarkable that the amplitude of the drag and lift components is kept almost constant under the fully developed status.

2.3. Boundary conditions

The non-slip boundary condition is applied to the cylinder surface (and slit walls). Uniform free stream velocity is applied to the inlet of computational domain: $u = U_\infty$ and $v = 0$. $\partial u/\partial x = 0$ and $\partial v/\partial x = 0$ are applied at the exit of computational domain. Symmetry boundary conditions, $\partial u/\partial y = 0$ and $v = 0$, are applied at the upper and lower computational domain.

2.4. Numerical methods

The N-S equations are discretized using finite volume method, that is integral form of the conservation equations is solved in control volumes, which form a partition of the computational domain. Second order upwind scheme (discretizing the convective terms) and central difference scheme (the diffusive terms) are used. The second order implicit method is used for temporal discretization. The SIMPLE (Semi-Implicit Method for Pressure-Linked Equations) algorithm proposed by Patankar and Spalding (1972) [48] is applied to solve the pressure-velocity coupling. The Crank-Nicholson scheme is applied for the discretization of the time term. In the present work, convergence is verified if each residual of the above-mentioned equations is smaller than 10^{-6}.

3. Validation

3.1. Grid convergence test

A non-uniform grid distribution with dense clustering of grid points in the regions having high gradients of parameters and coarser grids in the regions with low gradients of parameters are used. Grid convergence is performed to test the mesh dimensions chosen for the case under consideration. The test case of flow over an unmodified cylinder at Re = 200 is chosen to validate the spatial discretization. The grid sensitivity analysis is performed using four different grid sizes to be compared with the selected one. The grid discretization in the cylinder zone (zone 5) for all the test cases is $N \times N = 30 \times 30$, 40×40, 50×50, 60×60, and 70×70, where 60×60 is the selected mesh resolution. The information of the test cases is given in Table 1, where L is the number of nodes along the cylinder surface. Taking the drag coefficient of the selected mesh resolution, M4 ($N \times N = 60 \times 60$), as a reference, deviation (absolute value) of the mean drag coefficient in different test cases with respect to mesh sizes is displayed in Figure 3. It can be observed that as the mesh size reduces from M4 to M5, the drag force changes slightly at a convergence order of 10^{-4}. Thus, we chose M4 as the most appropriate mesh resolution for the model considered.

Richardson extrapolation [49] is applied to test the order of accuracy by using three grid resolutions

Table 1. Meshing features of the test cases.

Meshes	M1	M2	M3	M4	M5
$N \times N$	30×30	40×40	50×50	60×60	70×70
L	120	160	200	240	280
Total cell volumes	15774	31328	43978	61648	79196

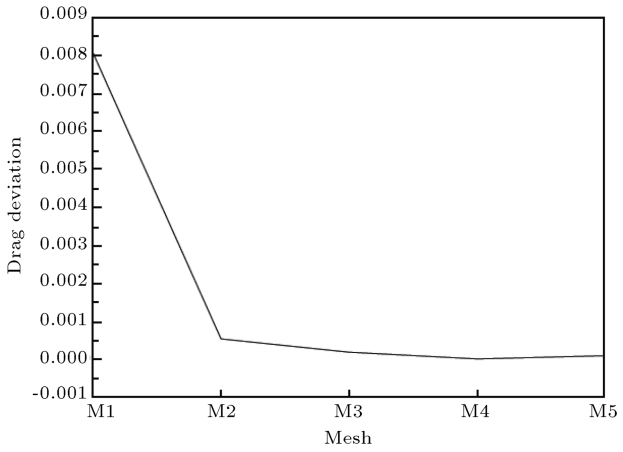

Figure 3. Drag deviation for different mesh sizes.

(M2, M3, and M4). Roache [50] generalized Richardson extrapolation by introducing the pth-order method:

$$f_{\text{exact}} \approx f_1 + [(f_1 - f_2)/(r^p - 1)], \tag{9}$$

where f_{exact} is the exact solution and r is the grid refinement ratio. Considering the three mesh resolutions, the following is observed:

$$f_2 - f_1 = \frac{(f_3 - f_2)}{r_{32}^p - 1} - \frac{(f_2 - f_1)}{r_{21}^p - 1}, \tag{10}$$

in which f_1, f_2, and f_3 represent computed mean drag force in case M4, M3, and M2, respectively, and $r_{32} = 40/50 = 0.8$ and $r_{21} = 50/60 = 0.8333$. Finally, we obtained result of $p = 1.87$, which is close to 2, and it is consistent with the second order accuracy of the discretization.

3.2. Validation of the code

Computational Fluid Dynamics software Fluent 6.3 is used in the present numerical simulation. There are no available results in literature to verify the present ones. Thus, it is necessary to confirm the accuracy of the present numerical simulation of flow past a circular cylinder; the results gained from an unmodified cylinder at Reynolds numbers from 60 to 200 are compared with available results to verify those of the present work. The numerical validations are mainly focused on the time-averaged drag coefficient C_D^M, amplitude of lift coefficient, C_L^A, and shedding frequency St.

The comparisons of parameters mentioned above with existing literature are shown in Tables 2-4. It can be observed that these characteristic values are in accordance with others' studies.

Table 2 shows the comparison of the computed mean drag coefficient C_D^M with available results, which

Table 2. Comparisons of mean drag coefficient C_D^M with literature at different Reynolds numbers.

Re	60	80	100	150	200
Present	1.426	1.375	1.348	1.330	1.342
He et al. (2000) [52]	1.39	1.35	1.35	···	1.36
Henderson (1995) [53]	1.42	1.37	1.35	1.33	1.34
Baranyi and Lewis (2006) [46]	1.41	1.36	1.34	1.33	···
Lu et al. [47]	1.41	1.37	1.35	1.33	1.34

Table 3. Comparisons of amplitude of lift coefficient C_L^A with literature at different Reynolds numbers.

Re	60	80	100	150	200
Present	0.150	0.260	0.350	0.530	0.700
Lu et al. (2011) [47]	0.14	0.25	0.34	0.53	0.69
Baranyi and Lewis (2006) [46]	0.13	0.24	0.32	0.51	···
Farrant et al. (2001) [54]	···	···	0.33	···	0.71
Linnick and Fasel (2005) [55]	···	···	0.34	···	0.70
Zhang et al. (2008) [56]	···	···	0.34	···	0.66
Le et al. (2008) [58]	···	0.26	···	···	0.68
Wang et al. (2009) [59]	···	0.26	···	···	0.71

Table 4. Comparisons of Strouhal number, St, with literature at different Reynolds numbers.

Re	60	80	100	150	200
Present	0.138	0.158	0.170	0.187	0.195
Lu et al. (2011) [47]	0.137	0.154	0.165	0.184	0.196
Wang et al. (2009) [59]	···	0.158	0.170	···	0.195
Williamson (1989) [60]	0.136	0.152	0.164	0.179	0.183
He et al. (2000) [52]	0.135	0.153	0.167	···	0.198

indicates good consistency. In general, the mean drag force is found to reduce as the Reynolds number augments. The cause is the decline of the viscous contribution which plays a role for the total drag force within the laminar flow regime [51]. The comparison of the amplitudes of fluctuating lift coefficient C_L^A at various Reynolds numbers is displayed in Table 3. Good agreements between the present work and other's numerical results are observed as well. Different from the drag force, the amplitude of lift fluctuation is observed to increase rapidly as the Reynolds number augments. Finally, the numerical validation of the Strouhal number is presented in Table 4. The good agreements between the computed results of the present work and the available numerical and experimental data also confirm that the present numerical model works well. It can be found that the Strouhal number augments gradually as the Reynolds number increases, suggesting that the period of vortex shedding from a bluff body in the laminar flow regime may be prolonged at lower Reynolds number. To this point, it is necessary to realize that the lift force reflects two important fundamental characteristics of flow past a bluff body. One is the pressure distribution nearby the fluid-solid interface and the other is the Strouhal number. The former correlates closely to the evolution of flow field, while the latter depends on the vortex shedding frequency.

4. Results and analysis

The model is then applied to probe the flow over modified cylinders. The effects of the slit width ratios on the flow over a cylinder are investigated. For unsteady laminar flow over a cylinder, the alternative shedding vortex yields the fluctuating forces, namely the drag force and lift force. Therefore, the drag and lift coefficients are two significant parameters which illustrate the variation of the flow field. The shedding frequency of the vortex is determined by the lift fluctuation, thus the Strouhal number, St, is calculated by the power spectrum of the lift coefficient. The effects of the slit width ratios on the variation of the drag, lift coefficients, and the shedding frequency at Re = 60, 80, 100, 150, 200, and 250 are investigated. The model of different slit width ratios used are $s/D = 0$, 0.10, 0.15, 0.20, 0.25, 0.30. Actually, the present configuration is derived from the cutting of the same cylinder. The difference among the present cases is due to the slit caused by different cutting. To simplify the description, the cases are to be referred to as S0, S1, S2, S3, S4, and S5, henceforth.

4.1. Drag forces

In this section, the mean drag coefficients are compared in the modified cases (with slit) with the corresponding value for unmodified case (without slit). Numerical simulations are carried out in the Reynolds number ranges from 60 to 250, and numerical results at Re = 150 and Re = 250 are specifically discussed.

The mean drag coefficients obtained numerically from the unmodified case (S0) are in good agreement with the values reported by other authors (Baranyi and Lewis [46], Lu et al. [47], He et al. [52], and Henderson [53], shown in Table 2). Figure 4 shows the variation of the drag coefficients with Reynolds numbers at different slit width ratios. A sharp reduction of the total drag coefficients could be observed as the slit width ratio increases at Re = 150 ∼ 250.

On the other hand, the decrease of the total drag forces is slight when the Reynolds number is relatively low. The maximum drag drop occurs in case S5 at Re = 250, with a drag reduction by 30.4%. The results presented demonstrate the effectiveness in improving the drag performance by slit modification.

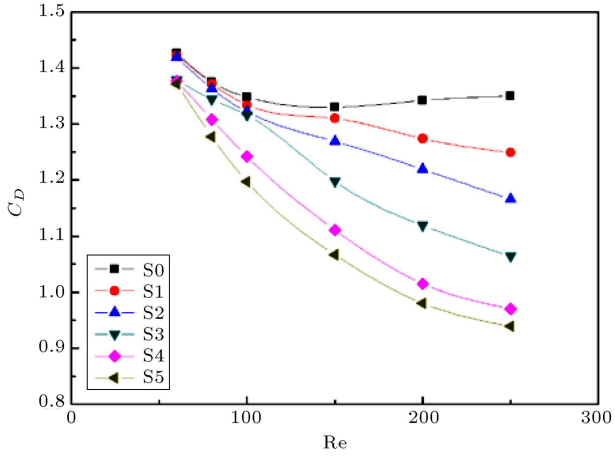

Figure 4. Variation of the mean drag coefficients with Reynolds numbers at different slit width ratios.

Table 5. Mean drag coefficients of all the modified cases at Re = 60 ∼ 250.

	Re					
s/D	60	80	100	150	200	250
0	1.426	1.375	1.348	1.330	1.342	1.350
0.10	1.423	1.372	1.334	1.310	1.274	1.249
0.15	1.419	1.363	1.322	1.269	1.219	1.166
0.20	1.379	1.344	1.316	1.198	1.119	1.064
0.25	1.377	1.308	1.242	1.111	1.015	0.970
0.30	1.362	1.277	1.197	1.067	0.980	0.939

Drag reduction performance of passive control method by placing a slit parallel to the flow direction was also found by Igarashi [31] and Olsen and Rajagopalan [32] in their experimental works. The decline of the total drag forces is caused by diminution of the pressure difference between the higher pressure in the front stagnation zone and the lower pressure in the rear separated zone, which is derived from diverting part of the fluid from the front stagnation point of the cylinder into the low pressure zone in the rear of the cylinder through an internal slit. The mean drag coefficients of all the modified cases at Re = 60 ∼ 250 are presented in Table 5.

The drag force is a result of the convective motion of the cylinder through the fluid. In viscous flow, the total drag force is contributed by the pressure and skin friction (or viscous) components. The pressure component causes a large drag contribution in total drag. The pressure and viscous contributions of the drag coefficient from steady and unsteady two-dimensional computations were determined by Henderson [53]. Figure 5 shows the total drag coefficients, pressure drag coefficients, and friction drag coefficients as the slit width changes at Re = 150 and Re = 250. It can be found that as the slit width increases, the contribution of pressure component declines, while the contribution of viscous component increases. The reduction of the pressure drag forces results from the fact that the slit-formed channel connects the front stagnation point and the rear low pressure zone of the cylinder, leading to the diminution of the pressure difference between the front stagnation zone and the rear separated one of the cylinder. On the other hand, the increase of the skin friction forces is attributed to the two sides added by the slit. The compensation of the pressure drag force reduction for the viscous force increase results in the decrease of the total drag force.

For flow over usual circular cylinder and cylinder with slit, a uniform Reynolds number $\mathrm{Re} = U_\infty D/\nu$ is defined. Next, we will discuss the Reynolds number, if it is recalculated because of the existence of slit in modified cylinders. For modified cylinders, the crosswise length as seen from the stream has been changed in consequence of the slit across the cylinder. A new Reynolds number, $\mathrm{Re}' = U_\infty D'/\nu$, is defined, in which D' is the crosswise length as seen from the stream considering slit width. Then, we will get five new Reynolds numbers (Re′) for every Re (because the Reynolds number is recalculated due to five slit widths). A comparison study at Re = 150 is carried out to explore whether the modified cylinders (with slit) are still interesting when the Reynolds numbers are updated. Table 6 displays computed results, C_D^M, for Re = 150 in different cases and mean drag coefficient, $C_D^{M\prime}$, at corresponding Re′ for unmodified cylinders. It could be observed that even though the Reynolds number is recalculated, the drag reduction feature of the modified cylinder is still satisfied. Another feature which deserves to be mentioned is that in the

Table 6. Drag reduction performance of modified slit model at Re′.

s/D	Re′	$C_D^{M\prime}$	C_D^M
0	150	1.330	1.330
0.10	135	1.331	1.310
0.15	127.5	1.333	1.269
0.20	120	1.335	1.198
0.25	112.5	1.338	1.111
0.30	105	1.344	1.067

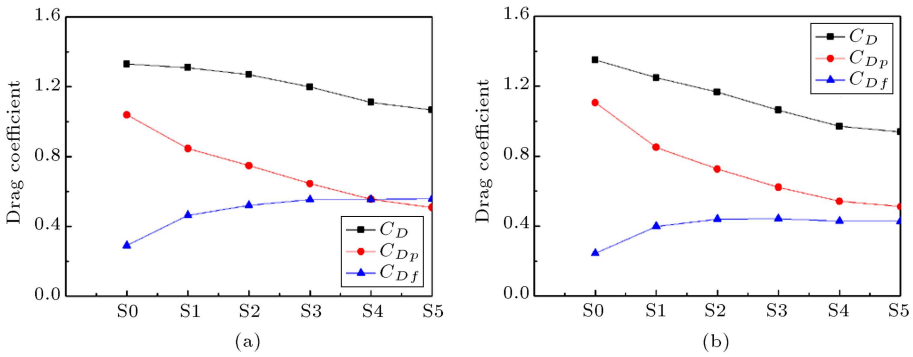

Figure 5. Total drag coefficients, pressure coefficients, and friction coefficients at different control cases: (a) Re = 150; and (b) Re = 250.

considered Reynolds number range, the average drag coefficient of flow over usual cylinder changes slightly (which could be referred to the work of Rajani et al. [51]). However, the percentage of drag reduction of the modified cylinder is significant. To set a uniform criterion to evaluate the drag and lift forces as well as the vortex shedding structures for different control models, we still use the common Reynolds number definition for the following discussions.

4.2. Lift forces and shedding frequency

Vortex shedding from the upper and lower surfaces of the circular cylinder generates periodic pressure fluctuations around the circular cylinder. The fluctuating lift force is mainly due to the fluctuating pressures acting on the surface of the cylinder [18]. When the shear layer is being shed downstream from one side of the surface, a low pressure region is evolved on that side, while a high pressure region is evolved on the opposite side. The phenomenon continues alternately, and hence, unsteady lift fluctuations are experienced by the bodies at the frequency of the vortex shedding (f_S) [57], that is, the lift fluctuation energy is concentrated on a band around f_S. The Strouhal number St is a non-dimensional transformation of the shedding frequency f_S. The time traces of the fluctuating lift coefficient in different cases are presented in Figure 6.

The amplitude of lift fluctuation is greatly reduced with the increase of the slit width at Re = 150, with a maximum reduction to an order of 10^{-4}, as shown in Figure 7. Similar results could be found at Re = 60, 80, and 100. However, a different feature of the C_L variation is found at Re = 250. As the slit width ratio increases to 0.20 (S3), a positive value of the mean lift force could be found and the mean lift force is negative in the case S4. At the maximum slit width ratio of $S/D = 0.30$ (S5), a periodic oscillating lift force appears again, as shown in Figure 6. It is due to the onset of the vortex shedding from the slit. The phenomenon will be further discussed in the flow field section by displaying the vortices contours. The shedding frequencies are determined by the lift coefficient fluctuation. The Strouhal number, St, is captured with the power spectral analysis of C_L, as shown in Figures 8 and 9. The obtained Strouhal numbers of Re = 150 and Re = 250 will be discussed separately. Figure 8 displays the FFT of the lift histories, the resulting Strouhal number, and corresponding power spectral density at Re = 150. A significant drop of the power spectral density could be observed as the slit width ratio increases; however, the shedding frequency changes slightly from S0 to S3; while in cases S4 and S5, a favorable reduction of the St is observed, declining from 0.187 of case S0 to 0.162 in case S4 and 0.145 in case S5, respectively. When Re is equal to 250, a St = 0 is found in cases S3 and S4 due to the disappearance of the lift fluctuation, while in case S5, a secondary frequency is observed, which is the result of the existence of the vortices shedding from the slit (as shown in Figure 9).

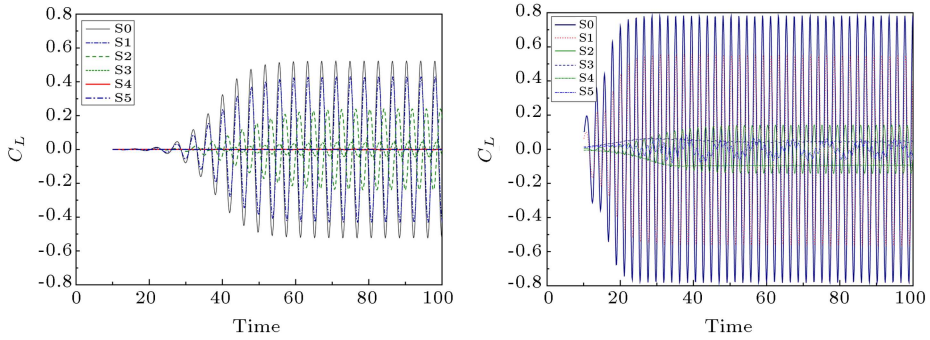

Figure 6. Time histories of the lift coefficient in different modified cases at Re = 150 and Re = 250.

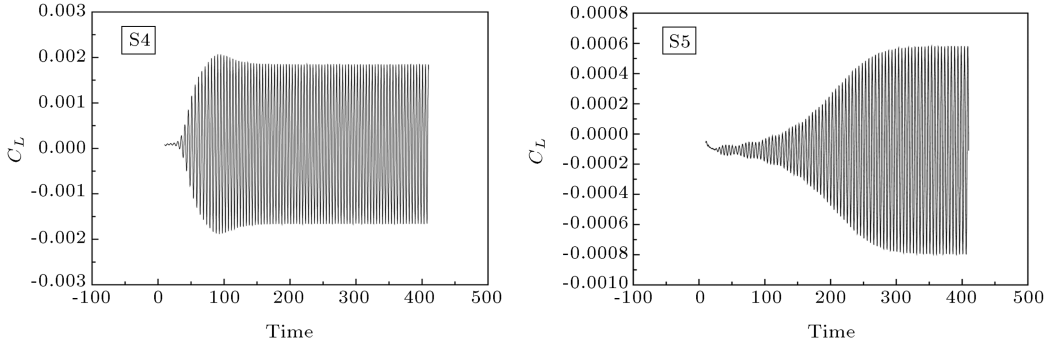

Figure 7. Time histories of the lift coefficient of cases S4, and S5 at Re = 150.

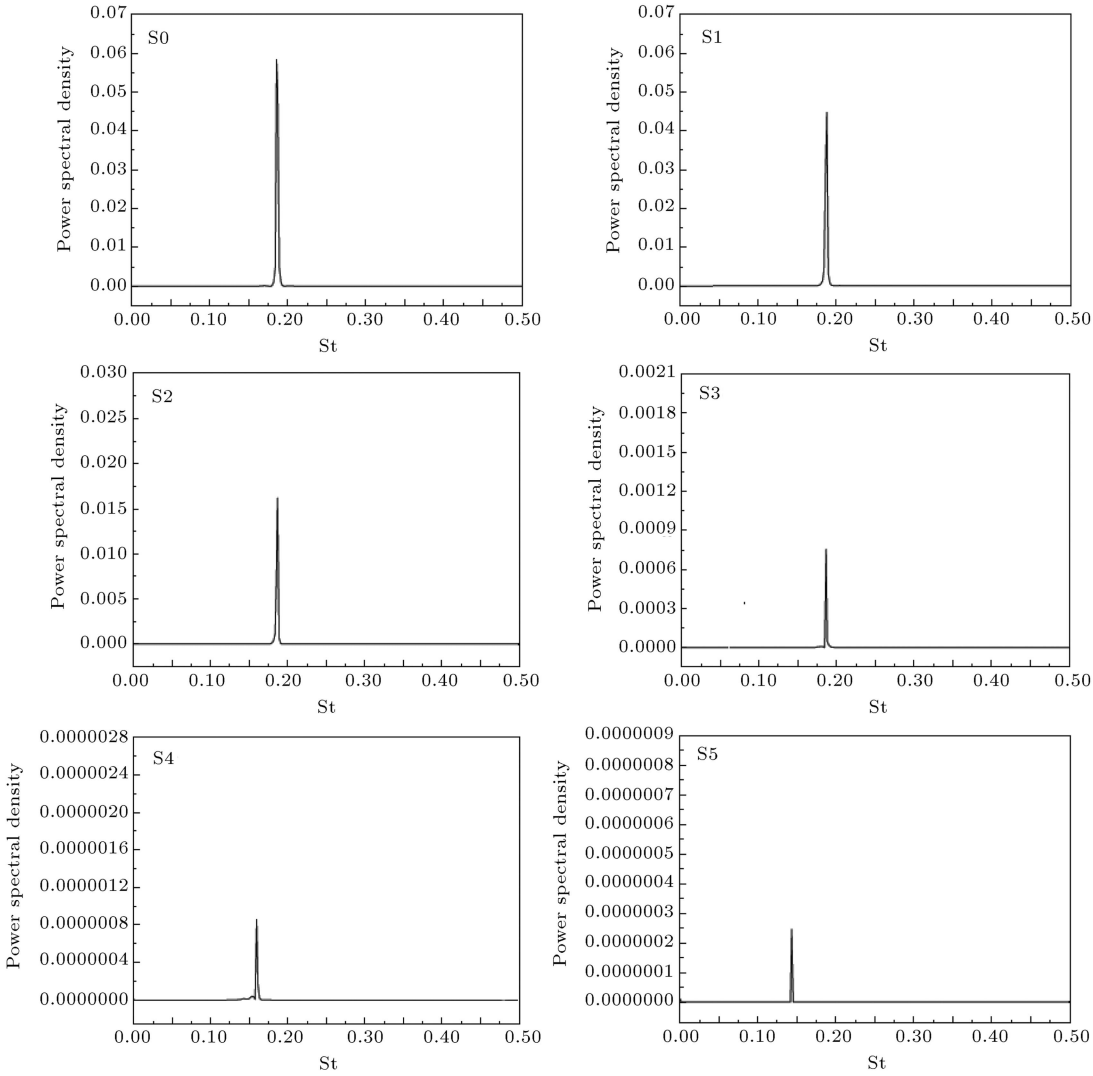

Figure 8. Strouhal number and power spectral density at Re = 150.

4.3. Flow field

The unsteady flow over a circular cylinder is initiated by the separated boundary layers that naturally become unstable beyond the first critical Reynolds number. The separation point is located at the surface of the cylinder, where the shear stress is zero. As the separation angle varies during the period of vortex shedding, the separation position is derived from the flow field. The shear stress at the cylinder surface is obtained from the tangential velocity gradient along the radius of the cylinder, namely $\partial u_\tau/\partial n$. At the location ahead of a special position of the cylinder wall, the distribution of boundary layer velocity, $\partial u_\tau/\partial n$, is positive. The positive pressure gradient in the circumferential direction (adverse pressure) will result in the decrease of $\partial u_\tau/\partial n$. If the adverse pressure gradient persists, $\partial u_\tau/\partial n$ will be zero at a position, and the flow will be separated from the boundary. For the unmodified cylinder, the separated shear layers are deflected inwards immediately after passing the separation point, and a back flow occurs in the downstream separation, forming the well-known Karman vortex. The numerical results show that the slit through the cylinder has altered the evolution of vortex formation significantly in the cylinder wake. In the cylinder-slit configuration, the free shear layers roll up further downstream progressively from the cylinder as the size of the slit increases. The phenomenon mentioned above could be explained by the following facts that with the expansion of the slit width, the fluid quantity flowing through the slit increases, and vortex shedding from the slit could hinder the interaction between the top and bottom vortices forming the cylinder surface, thus rolling up occurs where the shear layers have had more opportunity to diffuse, resulting in less compact vortex cores. Such shed vortices are less efficient in generating large pressure variations between the upper and lower sides of the cylinder, causing the observed decrease in drag and lift forces.

Figures 10 and 11 show time-dependent vorticity

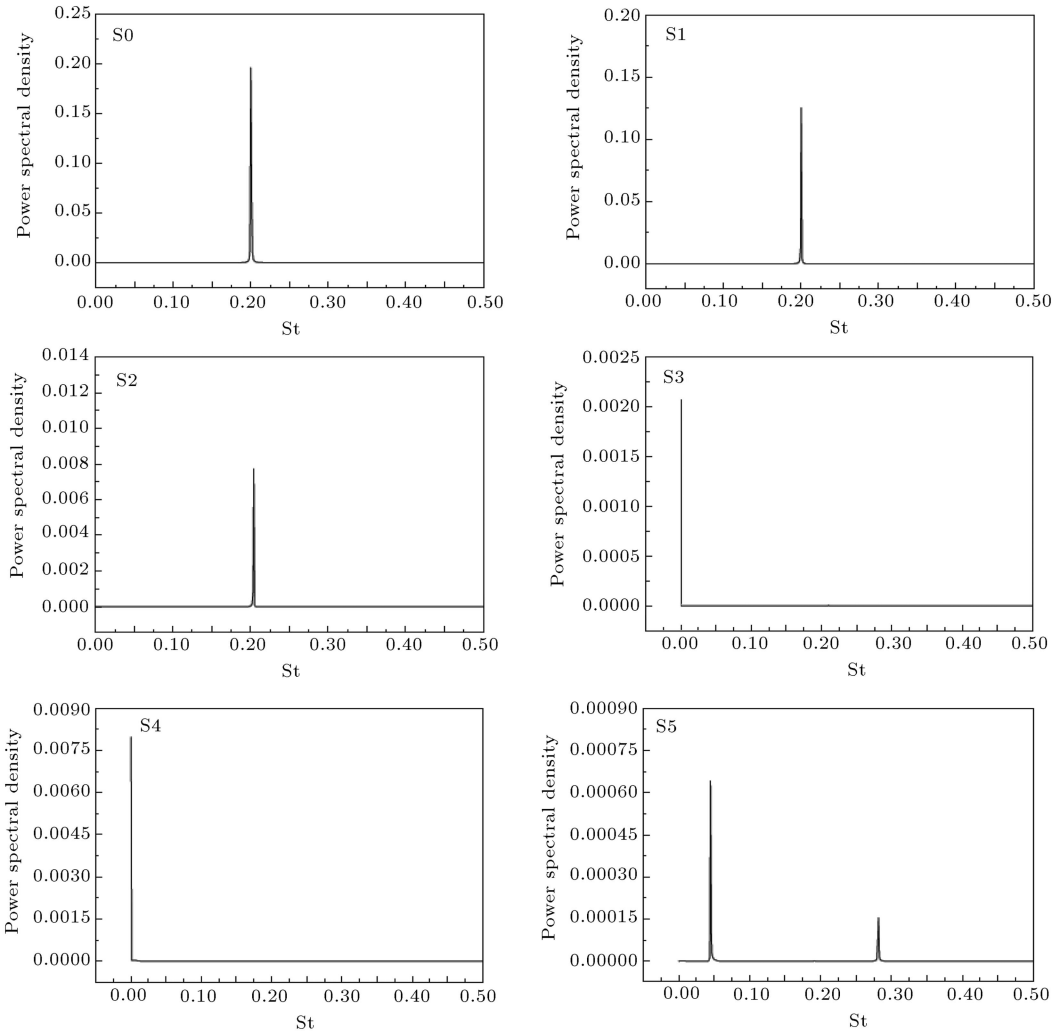

Figure 9. Strouhal number and power spectral density at Re = 250.

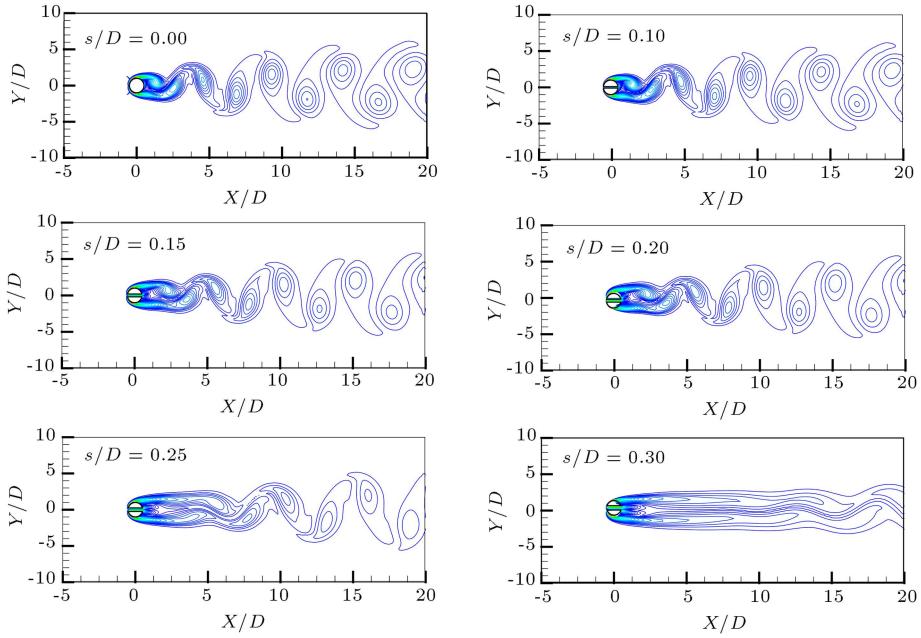

Figure 10. Instantaneous vorticity contour of flow past modified and unmodified cylinders at Re = 150.

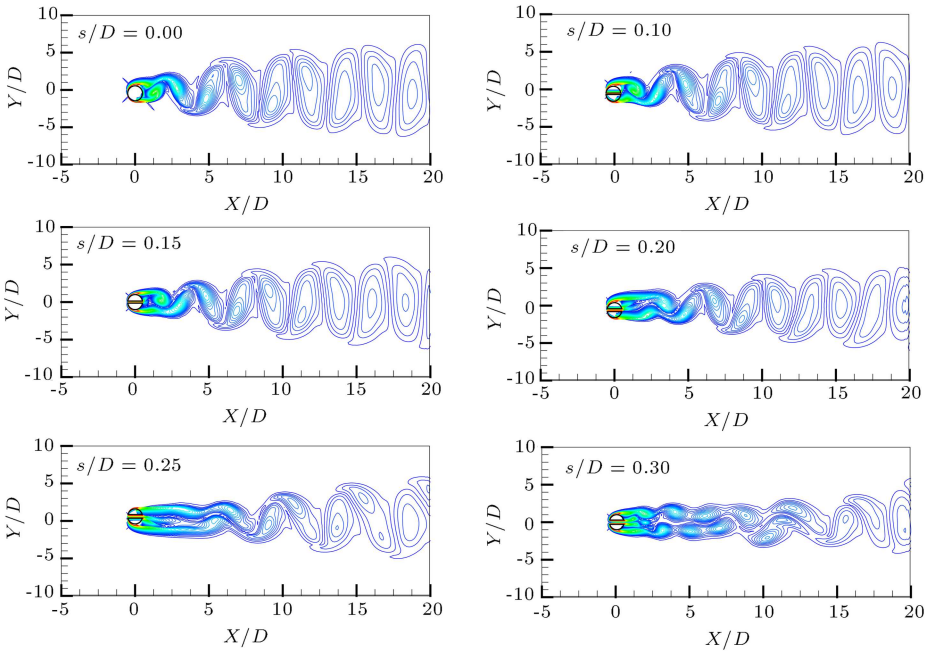

Figure 11. Instantaneous vorticity contour of flow past modified and unmodified cylinders at Re = 250.

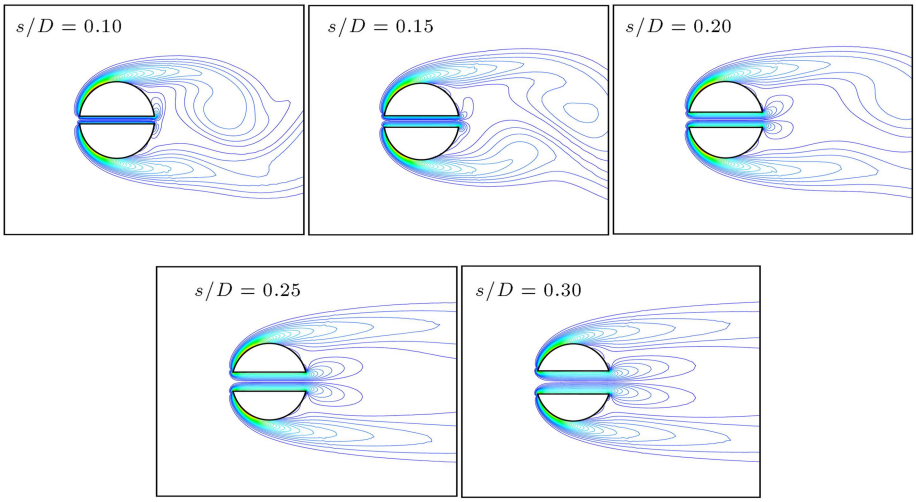

Figure 12. Close-up view of the vorticity contour of flow past modified cylinders at Re = 150.

contours of the entire flow field for all cases at Re = 150 and Re = 250. Detailed displays of the vortex shedding near the slit corresponding to Figures 10 and 11 are presented in Figures 12 and 13. It is obvious that the wake flow behind the cylinder is strongly affected by the slit. The most interesting feature is the appearance of the vortices generated from the slit with the expansion of the slit width, which impedes the interaction between the upper and lower shedding shear layers. Thus, the fluid through the slit drives the vortex formation region downstream and changes the anti-symmetric feature of the vortex shedding from the cylinder wall. Therefore, a suppression of the vortex shedding could be obtained by the modified slit method. Detailed analysis of the wake flow field will be presented in the following paragraphs.

First, the flow field of cylinder-slit flow at Re = 150 is displayed, as shown in Figure 10. For small slit ratio up to $s/D = 0.10$ (S1), the vortex shedding feature is slightly different from that of a cylinder without a slit (S0). As the slit width becomes larger, the rolling up of the separated shear layers is extended backwardly. As a consequence, the vortex formation region is pushed downstream due to the appearance of the slit vortices, which could be observed clearly in Figure 12. The vortices caused by the slit hinder the interaction between the upper and lower shear layers separated from the cylinder and delay the furling of the separated shear layers. In

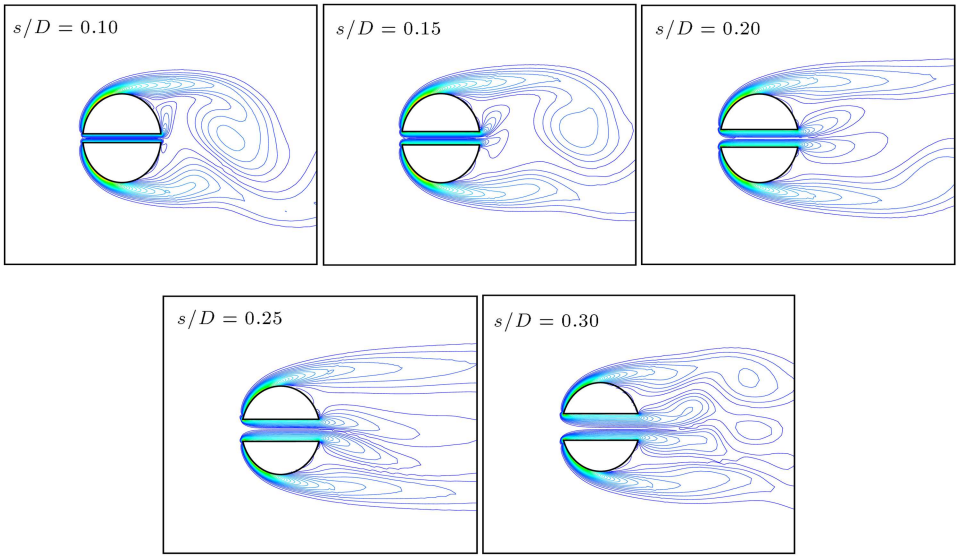

Figure 13. Close-up view of the vorticity contour of flow past modified cylinders at Re = 250.

case S5, the vortex's formation region behind the cylinder is driven downstream farthest when the lift force is minimum (at an order of 10^{-4}), as shown in Figure 7.

Next, we pay particular attention to the modified cases at Re = 250, as shown in Figure 11. For small slit ratios up to $s/D = 0.10$, the same phenomenon is observed as that at Re = 150. Cases S2, S3, and S4, however, show more different vortex structures. Partial enlarged drawings of the vorticity contour near the slit are displayed in Figure 13. As a result of the formation of stronger slit vortices, the slit vortices are biased towards either upper side or lower side, sporadically, resulting in mean value of the lift coefficient of 0.045 (S3) and -0.095 (S4), as shown in Figure 6. The flow pattern is similar to the biased bi-stable flow happened in flow past side-by-side cylinders when the distance between two cylinders is small [33]. However, for modified cases at Re = 150, the slit vortices only help to elongate the shear layer and will not interact with cylinder vortex. In the case S5, noticeable oscillating of the vortex shedding from the cylinder surface occurs again ($C_L = -0.06 \sim +0.06$). The cause is that vortices formed by the slit shed interact with the shear layers separated from the cylinder surface. The small scale secondary vortex generated at the rear edge of the slit (case S5, shown in Figure 13), which provides additional perturbations to the separated shear layers, results in the re-emergence of the fluctuating lift forces (as shown in Figure 6). Another corresponding result is the appearance of a secondary shedding frequency as shown in Figure 9.

In order to get a deeper insight on how the slit width will influence the flow structure if the slit width continually increases, we add three new modified cases, that is, $s/D = 0.35$, 0.40, and 0.45. The instantaneous vorticity contour of the new cases is displayed in Figure 14.

It can be observed that for the case of Re = 150, flow structures with larger slit width are similar to those of $s/D = 0.30$, proving that the structure shown in Figure 14(a) is the most stable state at this Reynolds number. Modified cases of $s/D = 0.35$ and $s/D = 0.40$ show similar vortex structures with those of $s/D = 0.30$ under the condition that Re = 250. Secondary vortices shedding from the rear edge of slit would interact with the vortices shedding from the cylinder surface. However, for the case of $s/D = 0.45$, both the main vortex shedding from the surface of the cylinder and the secondary one from the rear edge of slit disappear; the wake flow structure tends to be more stable. Therefore, we can come to the conclusion that in the laminar regime, the slit width of the optimal modified cylinder increases with the augmentation of Reynolds number.

5. Conclusions

A passive flow control method is proposed in the present work to reduce the fluctuating forces acting on the cylinder surface and suppress vortex shedding in the low Re number laminar region. The effect of the width of the slit placed along the cylinder diameter parallel to the incoming flow is numerically studied. Simulations are performed at a Reynolds number range of 60 to 250. The time traces of drag and lift coefficients, the Strouhal numbers, and flow features are comprehensively presented and compared with different modified cases in order to reveal the impact of slit width ratios on the behavior of the circular cylinder wake flow. It is shown that the nature of the vortex shedding evolution is significantly altered by the slit through the cylinder. In the

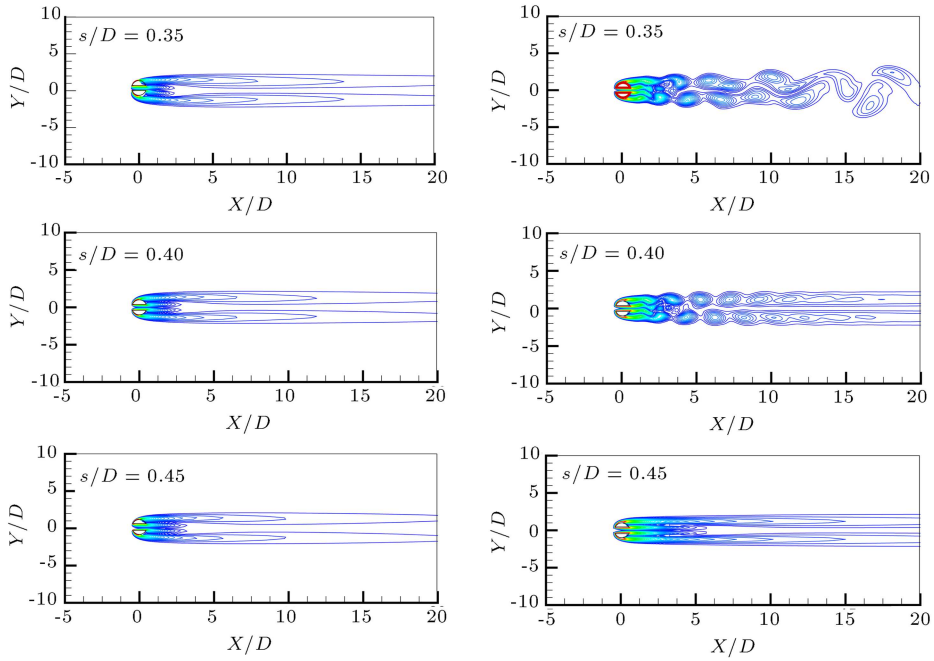

(a) Re = 150 (b) Re = 250

Figure 14. Instantaneous vorticity contour of flow past cylinders with larger slit.

comparison of the modified cylinders with conventional one, particular attention is paid to numerical results obtained at Re = 150 and Re = 250. The reduction of the drag force is caused by the inner duct formed by the slit which directs part of the fluid in the front stagnation region to the rear stagnation region and consequently decreases the pressure difference between the front stagnation and rear separated region. The lift coefficient also declines as the slit width increases at Re = 60 ∼ 200. The slit placed parallel to the flow direction also prolongs the formation of wake vortex. A very interesting vortex pattern found in the modified case is the vortex shedding of the slit and its interaction with the cylinder vortices, which contributes to the delay of the boundary layer separation. In conclusion, the modified slit method, which does not require an additional expenditure of energy, is a promising technique for drag reduction and vortex shedding suppression.

Acknowledgement

The authors gratefully acknowledge the financial support by the National Nature Science Fund of China (No. 50476063).

Nomenclature

D	The diameter of the cylinder;
F_D	Drag forces;
C_D	Drag coefficients;
C_D^M	Time-averaged drag coefficient;
St	Strouhal number;
p	Pressure;
f_s	Shedding frequency of the vortex;
U_∞	The free-stream velocity;
F_L	Lift forces;
C_L	Lift coefficients;
C_L^A	Amplitude of lift coefficient;
Re	Reynolds number;
u, v, x, y	Velocity components;
x, y	Coordinate direction.

Greek symbol

ν	Kinematic viscosity of fluid;
θ	Angle between the front stagnation streamline and a vector normal to the cylinder surface;
ρ	Density of fluid;
τ_w	Shear stress;
τ	Time.

References

1. Williamson, C.H.K. "Vortex dynamics in the cylinder wake", *Annu. Rev. Fluid Mech.*, **28**, pp. 477-539 (1996).
2. Behara, S. and Sanjay, M. "Wake transition in flow past a circular cylinder", *Physics Fluids*, **22**(11), pp. 114104.1-114104.11 (2010).

3. Qu, L., Norberg, Ch., Davidson, L., Peng, SH. et al. "Quantitative numerical analysis of flow past a circular cylinder at Reynolds number between 50 and 200", *Journal of Fluids and Structures*, **39**, pp. 347-370 (2013).

4. Williamson, C.H.K. and Govardhan, R. "Vortex-induced vibration", *Annu. Rev. Fluid Mech.*, **36**, pp. 413-455 (2004).

5. Roshko, A. "Perspectives on bluff body aerodynamics", *J. Wind Eng. Industr. Aerodyn.*, **49**(1-3), pp. 79-100 (1993).

6. Choi, H., Jeon, W.P. and Kim, J. "Control of flow over a bluff body", *Annu. Rev. Fluid Mech.*, **40**(1), pp. 113-139 (2008).

7. Wang, J.S., Xu, Y.X. and Tian, Y.S. "Active control of circular cylinder flow by affiliated rotating cylinders", *Sci. China Tech. Sci.*, **56**(5), pp. 1186-1197 (2013).

8. Muralidharan, K., Muddada, S. and Patnaik, B.S.V. "Numerical simulation of vortex induced vibrations and its control by suction and blowing", *Applied Mathematical Modeling*, **37**(1-2), pp. 284-307 (2013).

9. Chen, W.L., Xin, D.B., Xu, F. et al. "Suppression of vortex-induced vibration of a circular cylinder using suction-based flow control", *Journal of Fluids and Structures*, **42**(4), pp. 25-39 (2013).

10. Bao, Y. and Tao, J. "Active control of a cylinder wake flow by using a streamwise oscillating foil", *Phys. Fluids*, **25**(5), pp. 416-423 (2013).

11. Subhash Reddy, M., Muddada, S. and Patnaik, B.S.V. "Flow past a circular cylinder with momentum injection: optimal control cylinder design", *Fluid Dyn. Res.*, **45**(1), pp. 15501-15527 (2013).

12. Tang, S. and Aubry, N. "On the symmetry breaking instability leading to vortex shedding", *Phys. Fluids*, **9**, pp. 2550-2561 (1997).

13. Wehrmann, O.H. "Reduction of velocity fluctuations in a Karman vortex street by a vibrating cylinder", *Phys. Fluids*, **8**(4), pp. 760-761 (1965).

14. You, D., Choi, H., Choi, M.R. et al. "Control of flow induced noise behind a circular cylinder using splitter plates", *AIAA J.*, **36**(11), pp. 1961-1967 (1998).

15. Karniadakis, G.E. and Triantafyllou, G.S. "Frequency selection and asymptotic states in laminar wakes", *J. Fluid Mech.*, **199**, pp. 441-469 (1989).

16. Poncet, P. and Koumoutskakos, P. "Optimization of vortex shedding in 3D wakes using belt actuators", *Int. J. Offshore Polar Eng.*, **15**(1), pp. 7-13 (2005).

17. Poncet, P., Hildebrand, R., Cottet, G.-H., et al. "Spatially distributed control for optimal drag reduction of the flow past a circular cylinder", *J. Fluid Mech.*, **599**, pp. 111-120 (2008).

18. Gozmen, B., Akilli, H. and Sahin, B. "Passive control of circular cylinder wake in shallow flow", *Measurement*, **46**(3), pp. 1125-1136 (2013).

19. Lu, L., Liu, M.M., Bin, T., et al. "Numerical investigation of fluid flow past circular cylinder with multiple control rods at low Reynolds number", *Journal of Fluids and Structures*, **48**, pp. 235-259 (2014).

20. Oruc, V. "Passive control of flow structures around a circular cylinder by using screen", *Journal of Fluids and Structures*, **33**(5), pp. 229-242 (2012).

21. Bao, Y. and Tao, J. "The passive control of wake flow behind a circular cylinder by parallel dual plates", *Journal of Fluids and Structures*, **37**, pp. 201-219 (2013).

22. Rao, A., Thompson, M.C., Leweke, T., et al. "The flow past a circular cylinder translating at different heights above a wall", *Journal of Fluids and Structures*, **41**, pp. 9-21 (2013).

23. Schumm, M., Berger, E. and Monkewitz, P.A. "Self-excited oscillations in the wake of two-dimensional bluff bodies and their control", *J. Fluid Mech.*, **271**, pp. 17-53 (1994).

24. Strykowski, P.J. and Hannemann, H. "Temporal simulation of the wake behind a circular cylinder in the neighborhood of the critical Reynolds number", *Acta Mech.*, **90**(1), pp. 1-20 (1991).

25. Bearman, P. and Owen, J. "Reduction of bluff-body drag and suppression of vortex shedding by the introduction of wavy separation lines", *J. Fluids Struct.*, **12**(1), pp. 123-130 (1998).

26. Darekar, R.M. and Sherwin, S.J. "Flow past a square-section cylinder with a wavy stagnation face", *J. Fluid Mech.*, **426**, pp. 263-295 (2001).

27. Dobre, A., Hangan, H. and Vickery, B.J. "Wake control based on spanwise sinusoidal perturbations", *AIAA J.*, **44**(3), pp. 485-492 (2006).

28. Lee, S.J., Lim, H.C., Han, M. et al. "Flow control of circular cylinder with a V-grooved micro-riblet film", *Fluid Dyn. Res.*, **37**(4), pp. 246-266 (2005).

29. Yang, J.T., Yen, C.W. and Tsai, G.L. "Flame stabilization in the wake flow behind a slit V-gutter", *Combust. Flame*, **99**(2), pp. 288-294 (1994).

30. Tsuchiya, K. "The clouds with the shape of Karman vortex streets in the wake of Cheju Island", *Korea. J. Meteor. SOC. Japan*, **47**, pp. 457-465 (1969).

31. Igarashi, T. "Flow characteristics and a circular cylinder with a slit. 1st report, flow control and flow patterns", *Bulletin of JSME*, **21**(154), pp. 656-664 (1978).

32. Olsen, J.F. and Rajagopalan, S. "Vortex shedding

behind modified circular cylinders", *J. Wind. Eng. Ind. Aerodyn.*, **86**(1), pp. 55-63 (2000).

33. Zdravkovich, M.M. "Review of flow interference between two circular cylinders in various arrangements", *ASME Journal of Fluids Engineering*, **99**(4), pp. 618-633 (1977).

34. Zdravkovich, M.M. "The effects of interference between circular cylinders in cross flow", *Journal of Fluids and Structures*, **1**(2), pp. 239-261 (1987).

35. Bearman, P.W. and Wadcock, A.J. "The interaction between a pair of circular cylinders normal to a stream", *Journal of Fluid Mechanics*, **61**(3), pp. 499-511 (1973).

36. Kiya, M., Arie, M. and Tamura, H. "Vortex shedding from two circular cylinders in staggered arrangements", *ASME Journal of Fluids Engineering*, **102**(2), pp. 166-173 (1980).

37. Zdravkovich, M.M. "Flow induced oscillations of two interfering circular cylinders", *Journal of Sound and Vibration*, **101**(4), pp. 511-521 (1985).

38. Williamson, C.H.K. "Evolution of a single wake behind a pair of bluff bodies", *J. Fluid Mech.*, **159**, pp. 1-18 (1985).

39. Kim, H.J. and Durbin, P.A. "Investigation of the flow between a pair of circular cylinders in the flopping regime", *Journal of Fluid Mechanics*, **196**, pp. 431-448 (1988).

40. Wood, C. "The effect of base bleed on a periodic wake", *J. Roy. Aero. Soc.*, **68**, pp. 477-482 (1964).

41. Lin, J., Towfighi, J. and Rockwel, D. "Near-wake of a circular cylinder: control by steady and unsteady surface injection", *J. Fluids Struct.*, **9**(6), pp. 659-669 (1995).

42. Kim, J. and Choi, H. "Distributed forcing of flow over a circular cylinder", *Phys. Fluids*, **17**(3), pp. 033103.1-033103.16 (2005).

43. Baek, H. and Karniadakis, G.E. "Suppressing vortex-induced vibrations via passive means", *J. Fluids Struct.*, **25**(5), pp. 848-866 (2009).

44. Norberg, C. "Flow around a circular cylinder: aspects of fluctuating lift", *J. Fluids Struct.*, **15**(3-4), pp. 459-469 (2001).

45. Williamson, C.H.K. and Roshko, A. "Vortex formation in the wake of an oscillating cylinder", *J. Fluids Struct.*, **2**(4), pp. 355-381 (1998).

46. Baranyi, L. and Lewis, R.I. "Comparison of a grid-based CFD method and vortex dynamics predictions of low Reynolds number cylinder flows", *Aeronaut. J.*, **110**(1103), pp. 63-71 (2006).

47. Lu, L., Qin, J.M., Teng, B., et al. "Numerical investigations of lift suppression by feedback rotary oscillation of circular cylinder at low Reynolds number", *Phys. Fluids*, **23**(3), pp. 033601.1-033601.15 (2011).

48. Patankar, S.V. and Spalding, D.B. "A calculation procedure for heat, mass and momentum transfer in three-dimensional parabolic flows", *Int. J. Heat Mass Transfer*, **15**(10), pp. 1787-1806 (1972).

49. Richardson, L.F. and Gaunt, J.A. "The deferred approach to the limit. Part I. Single lattice, Part II. Interpenetrating lattices", *Phil. Trans. R. Soc. Lond., A1*, **226**(636-646), pp. 299-361 (1927).

50. Roache, P.J. "Perspective: A method for uniform reporting of grid refinement studies", *J. Fluids. Eng.*, **116**(3), pp. 405-413 (1994).

51. Rajani, B.N., Kandasamy, A. and Majumdar, S. "Numerical simulation of laminar flow past a circular cylinder", *Appl. Math. Model.*, **33**(3), pp. 1228-1247 (2009).

52. He, J.W., Glowinski, R., Metcalfe., R. et al. "Active control and drag optimization for flow past a circular cylinder I. Oscillatory cylinder rotation", *J. Comput. Phys.*, **163**(1), pp. 83-117 (2000).

53. Henderson, R.D. "Details of the drag curve near the onset of vortex shedding", *Phys. Fluids*, **7**(9), pp. 2102-2104 (1995).

54. Farrant, T., Tan, M. and Price, W.G. "A cell boundary element method applied to laminar vortex shedding from circular cylinders", *Comput. Fluids*, **30**(2), pp. 211-236 (2001).

55. Linnick, M.N. and Fasel, H.F. "A high-order immersed interface method for simulating unsteady incompressible flows on irregular domains", *J. Comput. Phys.*, **204**(1), pp. 157-192 (2005).

56. Zhang, X., Ni, S.Z. and He, G.W. "A pressure-correction method and its applications on an unstructured Chimera grid", *Comput. Fluids*, **37**(8), pp. 993-1010 (2008).

57. Gerrard, J.H. "An experimental investigation of the oscillating lift and drag of a circular cylinder shedding turbulent vortices", *J. Fluid Mech.*, **11**(2), pp. 244-256 (1961).

58. Le, D.V., Khoo, B.C. and Lim, K.M. "An implicit-forcing immersed boundary method for simulating viscous flow in irregular domains", *Comput. Methods Appl. Mech. Eng.*, **197**(25-28), pp. 2119-2130 (2008).

59. Wang, Z.L., Fan, J.R. and Cen, K.F. "Immersed boundary method for the simulation of 2D viscous flow based on vorticity-velocity formulations", *J. Comput. Phys.*, **228**(5), pp. 1504-1520 (2009).

60. Williamson, C.H.K. "Oblique and parallel modes of vortex shedding in the wake of a circular cylinder at low Reynolds number", *J. Fluid Mech.*, **206**, pp. 579-627 (1989).

Biographies

Wang Jian Sheng, PhD, is a Professor in the Department of Thermal Energy Engineering at School of Mechanical Engineering, Tianjin University, Tianjin, P. R. China. He received a BS degree in Power Machine and MS degree in Thermal Energy Engineering from Tianjin University, Tianjin, P. R. China, in 1984 and 1992, respectively, and a PhD degree in Fluid Mechanics from Tianjin University, Tianjin, P. R. China in 1995. His research interests include Computational Fluid Dynamics, Numerical Heat Transfer, Heat Transfer Enhancement, Flow Control, and Drag Reduction.

Wang Chen is a postgraduate in the Department of Mechanical & Mechatronics, University of Waterloo, Waterloo, Canada. He received his BS degree in Engineering Mechanics from Tianjin University, Tianjin, P. R. China, in 2015. His research interests include computational fluid mechanics and heat transfer.